Journal of Fluorine Chemistry 208 (2018) 65–72

Contents lists available at ScienceDirect

Journal of Fluorine Chemistry

journal homepage: www.elsevier.com/locate/fluor

Decomposition characteristics of $C_5F_{10}O$/air mixture as substitutes for SF_6 to reduce global warming

Yi Li[a], Xiaoxing Zhang[a,*], Song Xiao[a], Qi Chen[a], Dibo Wang[b]

[a] School of Electrical Engineering, Wuhan University, Wuhan 430072, China
[b] Electric Power Research Institute, China Southern Power Grid, Guangzhou 510623, China

ARTICLE INFO

Keywords:
$C_5F_{10}O$/air
Molecular dynamics
ReaxFF forcefield
SF_6 alternative gas

ABSTRACT

Sulfur hexafluoride (SF_6) is widely used in the power industry but is a serious greenhouse gas. Many researchers committed to achieving sustainable development of the power industry are finding alternatives to SF_6 gas. $C_5F_{10}O$ performs well in terms of environmental protection, insulation, and safety and is a potential environment-friendly alternative gas. In this paper, the insulation and decomposition characteristics of $C_5F_{10}O$/air gas mixture were examined using gas-insulation performance test platform, and decomposition products were detected by gas chromatography–mass spectrometry. The formation mechanism and distribution of $C_5F_{10}O$ decomposition products were analyzed through reactive molecular dynamics method and density functional theory. The influence of air on the decomposition of $C_5F_{10}O$ was also evaluated. Results showed that the decomposition of $C_5F_{10}O$/air gas mixture mainly produces $CF_3\cdot$, $C_3F_7\cdot$, $C_4F_7O\cdot$, CO, $CF_2\cdot$, $CF\cdot$, $F\cdot$ and CF_4. The breakdown voltage of $C_5F_{10}O$/air gas mixture decreased slightly after repeated breakdown tests, and CF_4, C_2F_6, C_3F_8, C_3F_6, C_4F_{10}, CF_2O were detected. These results can serve as a reference for the systematic comprehension of the decomposition characteristics of $C_5F_{10}O$/air gas mixture and for related engineering applications.

1. Introduction

Sulfur hexafluoride (SF_6) gas has excellent insulation and arc performance and has been widely used in the power industry. According to statistics, about 80% SF_6 in the world is used in various types of gas-insulated equipment in the power industry, such as high-voltage circuit breakers, gas-insulated lines (GIL) and so on [1]. However, SF_6 is a serious greenhouse gas, with its lifespan in the atmosphere exceeding 3200 years and greenhouse effect potential (GWP) that is 23,500 times that of CO_2 [2–4].The Kyoto Protocol explicitly listed SF_6 as one of the six restricted greenhouse gases in 1997 [5]. Over the past five years, SF_6 gas has grown in the atmosphere by 20%, and the constantly increasing greenhouse gas emissions will lead to an increase in global average temperatures of about 4 °C (Celsius degree) in 2100 [6,7]. In order to realize the coordinated and sustainable development of the power industry, and gradually eliminate the dependence on SF_6, searching for an environment-friendly SF_6 alternative gas as an insulating medium used in electrical equipment is of great urgency.

In the past two years, $C_5F_{10}O$ and its gas mixture have attracted attention in the field of alternative gas research. Its molecular structure is shown in Fig. 1. The GWP value of $C_5F_{10}O$ is only 1, and its ozone depression potential index (ODP) is 0. Although $C_5F_{10}O$ has a liquefaction temperature of up to 26.9 °C [8], its insulation performance is excellent with a dielectric strength twice than that of SF_6; thus it has the potential of reaching the insulation strength of SF_6 at the same atmospheric pressure by mixing with a low liquefaction temperature buffer gas such as CO_2, N_2, and air. Moreover, $C_5F_{10}O$ is nontoxic and has an occupational exposure limit time average of 225 ppm_v (parts per million). [8]. Therefore, $C_5F_{10}O$ has great properties in terms of environmental protection, insulation, and safety.

Several scholars tested the insulation performance of $C_5F_{10}O$ and its mixtures and found that $C_5F_{10}O$/air gas mixture has excellent insulation properties, and has potential use in medium-voltage and high-voltage electrical equipment [8–10]. For engineering applications, Asea Brown Boveri Ltd. (ABB) has developed a switch cabinet with $C_5F_{10}O$/air gas mixture as insulation medium. It has passed the relevant standard test of the International Electrotechnical Commission (IEC) and has been carried out in test run successfully [8].

To evaluate the performance of gas-insulated medium comprehensively, besides the insulation and arc extinguishing characteristics, the decomposition characteristics also need to be investigated. In long-term operations or fault conditions, the internal insulation defects of the equipment caused by aging will lead to partial discharge (PD) or flashover, resulting in the decomposition of gas insulation medium. For

* Corresponding author at: School of Electrical Engineering, Wuhan University, BaYi Street No.299, Wuhan, Hubei Province, China.
E-mail address: xiaoxing.zhang@outlook.com (X. Zhang).

https://doi.org/10.1016/j.jfluchem.2018.01.015
Received 17 December 2017; Received in revised form 27 January 2018; Accepted 30 January 2018
Available online 01 February 2018
0022-1139/

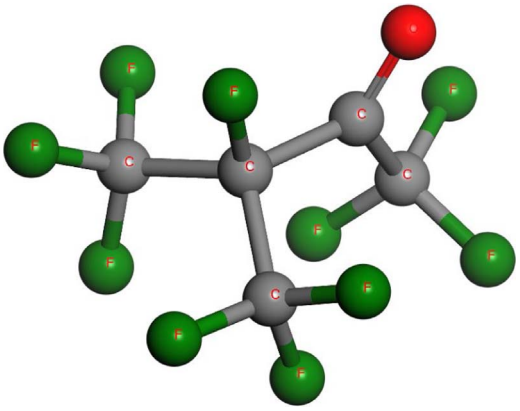

Fig. 1. Molecule structure of $C_5F_{10}O$.

example, the most widely used insulation medium, SF_6 can decompose and produce SO_2F_2, SO_2, SOF_2, and many other products [11]. The decomposition properties of gas insulating medium are closely related to its self-recovery characteristics, and the types of decomposition components also determine its safety. Therefore, the study of the decomposition characteristics of a new insulating medium needs to be done first, before engineering application.

At present, research on the decomposition characteristics of $C_5F_{10}O$ and its gas mixture have made some progress. Tatarinov et al. tested the decomposition of $C_5F_{10}O/N_2$ and $C_5F_{10}O$/air mixtures using dielectric barrier discharge (DBD) and found that the main products are C_4F_{10}, C_6F_{14}, C_5F_{12}, C_3F_6, and C_3F_8; and with the increase in applied voltage, the decomposition rate of $C_5F_{10}O$ increases. The decomposition rate of $C_5F_{10}O/N_2$ gas mixture is slower than that of $C_5F_{10}O$/air gas mixture at the same condition [12,13]. Hyrenbach et al. detected the composition of $C_5F_{10}O$/air gas mixture used in the switch cabinet as the insulating medium under long-term operation and internal arc faults by gas chromatography-mass spectrometry (GC–MS). Apparently, C_3F_7H and C_3F_6 are the main decomposition products under normal operating conditions. The components of CO, CO_2, CF_4, C_3F_8, and C_2F_6 are detected under internal arc tests [14]. Our team has calculated the possible decomposition paths of $C_5F_{10}O$ from the theoretical level and the effects of trace water were evaluated. The reaction enthalpy of each possible path, the ionization characteristics and toxicity of the decomposition products were analyzed [15,16]. We also studied the decomposition characteristics of $C_5F_{10}O/CO_2$ gas mixture and found that the main decomposition species are CF_3·and CO [17].

In this paper, the insulation and decomposition characteristics of $C_5F_{10}O$/air gas mixture were first tested using gas-insulation performance test platform and GC-MS. The decomposition mechanism of $C_5F_{10}O$/air gas mixture were theoretically explored by reactive molecular dynamics method (ReaxFF-MD) and density functional theory (DFT). The main decomposition paths and the influence of temperature on the reaction enthalpy were analyzed. Related research results provide a reference for a systematic and comprehensive understanding of the decomposition characteristics of $C_5F_{10}O$/air gas mixture and for related engineering applications.

2. Methods

2.1. Experimental method

The gas insulating performance test platform was used to conduct multiple breakdown tests on the $C_5F_{10}O$/air gas mixture, and the decomposition products were detected by GC-MS.

Fig. 2 shows the wiring diagram of the test system. The system consists of test transformers, protection resistors, capacitive voltage divider, and gas chamber. The transformer is used to provide high voltage; and the protective resistor is used to protect the test transformer, and to avoid the damage of the test transformer after overcurrent due to the breakdown. The capacitive divider is used to measure the actual voltage across the electrodes. The volume of the test chamber is 20 L; the main constituent material is 304 L stainless steel and polytetrafluoroethylene with excellent corrosion resistance, to avoid the chemical reaction between $C_5F_{10}O$ and gas chamber materials, and to ensure the accuracy of the composition test results.

The ball electrode, with radius of 25 mm and electrode interval of 5mm, was used to simulate a slightly non-uniform electric field. The electrode material is red copper. The electric field utilization coefficient is used to describe the electric fields with different uniformities, which is defined as $f = E_{av}/Emax$, where $Emax$ is the maximum electric field intensity, and E_{av} is the average electric field intensity [16]. The electric field utilization coefficient f of the ball electrode is 0.5168, hence, the electric field distribution between the ball electrode models is a slightly non-uniform electric field.

Before the test, the air tightness of the chamber was checked, and nitrogen was used to the wash the gas three times to eliminate the influence of the impurity in the air chamber. A mixture of 13.6% $C_5F_{10}O$, 69.12% N_2, and 17.28% O_2 is then added to 0.15 Mpa [14]. Then, the step-stress test (boost rate of about 0.5 kV/s) is used by applying the AC voltage to the positive and negative electrodes of the chamber until breakdown, and the instantaneous value of the breakdown voltage is recorded. The above test was repeated 30 times with an interval of 2 min. At the end of the test, the gas in the chamber was collected, and the gas components were tested by gas chromatography mass

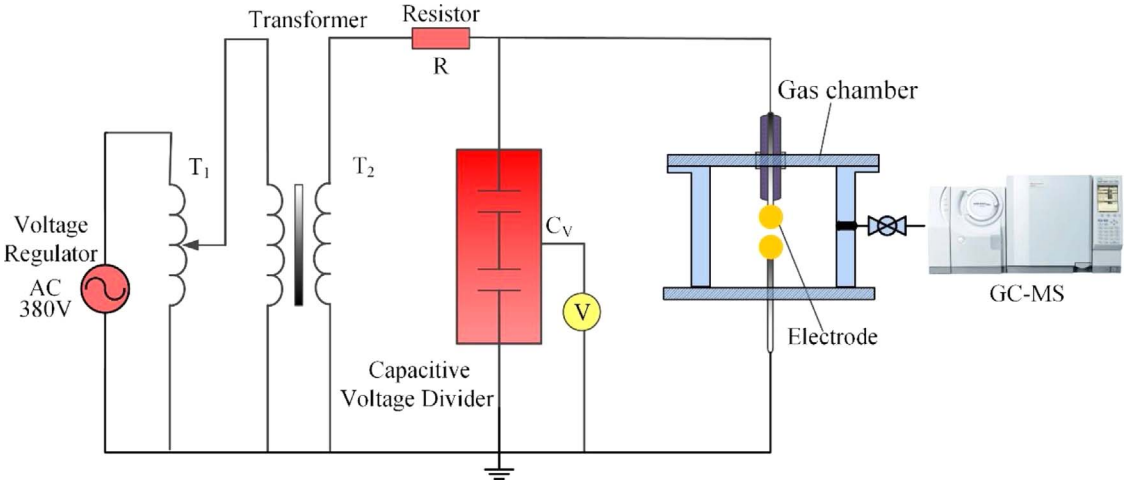

Fig. 2. Experimental system diagram.

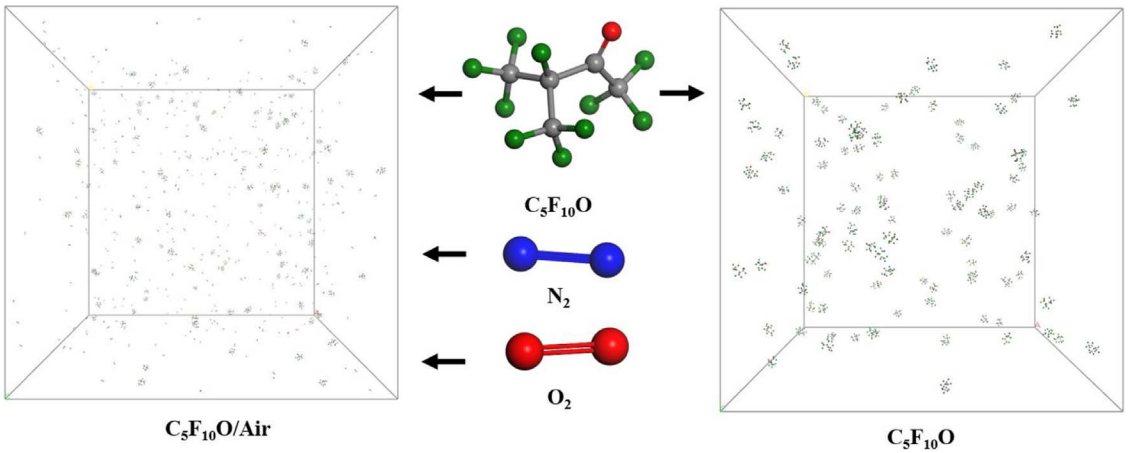

Fig. 3. Representative snapshots of $C_5F_{10}O$/air and $C_5F_{10}O$ systems.

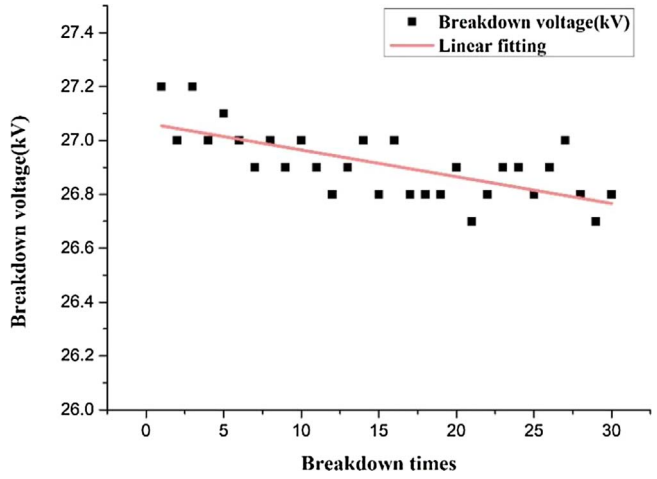

Fig. 4. Breakdown voltage at different breakdown times.

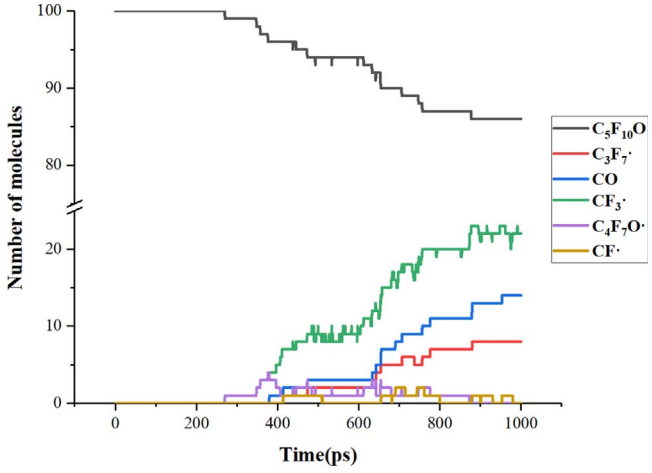

Fig. 6. Time evolution of $C_5F_{10}O$/air gas mixture and major products at 2600 K.

spectrometry (Shimadzu Ultra 2010plus with CP-Sil 5 CB column).

2.2. Calculation method

To further clarify the decomposition mechanism $C_5F_{10}O$/air mixture, both the ReaxFF-MD and DFT calculations were adopted. ReaxFF is a reactive force field method which uses the concept of bond order to model the interactions in a chemical system. ReaxFF overcomes the shortcomings of traditional molecular dynamics simulations that cannot simulate dynamic chemical reactions. It has been successfully applied in the chemical reaction kinetics simulation [18,19]. In ReaxFF force field, the energy function is described as follows [20],

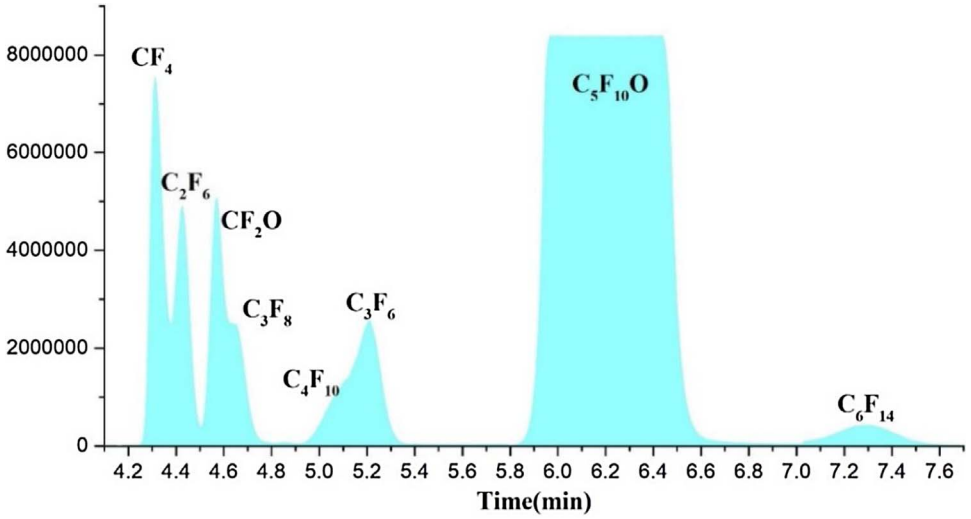

Fig. 5. Chromatogram of $C_5F_{10}O$/air gas mixture after breakdown test.

Table 1
Initial generation time and reaction paths of decomposition products.

Product	Generation temperature (K)	Generation time (ps)	Reaction path	ΔE (kcal/mol)[a]	
$C_4F_7O\cdot$,$CF_3\cdot$	2600	270.625	A	C5F10O → CF3•+C3F7CO•	78.71
$C_3F_7\cdot$,CO	2600	380	B	C5F10O → CF3•+C3F7•+CO	82.80
CF·	2600	414.375	C	C3F7CO• → 2CF3•+CF•+CO	138.45
$CF_2\cdot$	2600	740	D	CF3• → CF2• + F•	77.74
CF_4	3000	806.250	E	CF3• + F•→CF4	−103.53

[a] at mGGA-M06L level with ZPE correction and enthalpy correction at 2600 K.

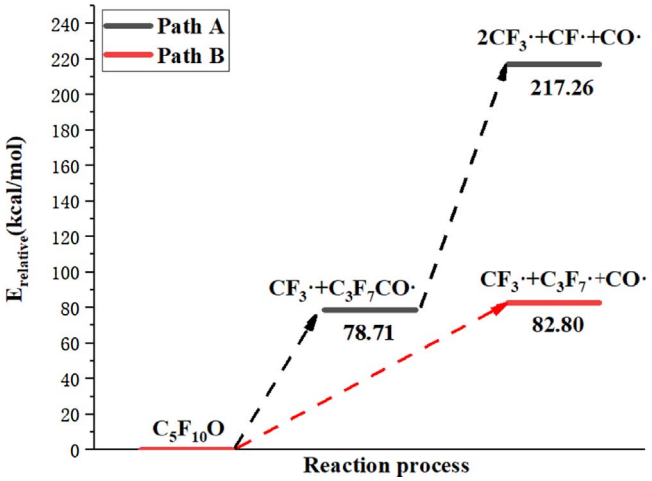

Fig. 7. Relative energy change of each decomposition paths (at mGGA-M06L level with ZPE correction and enthalpy correction at 2600 K).

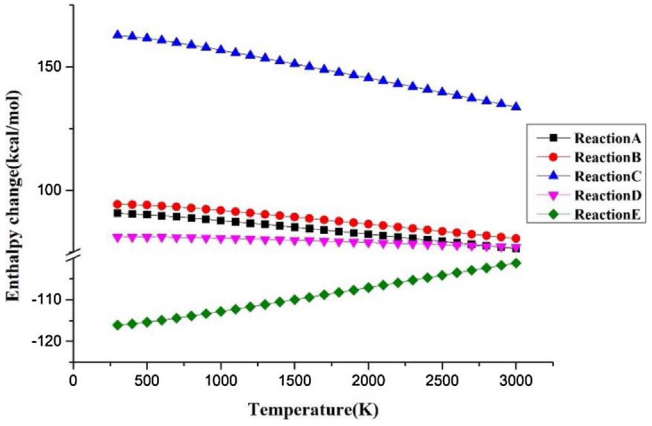

Fig. 8. Enthalpy change of decomposition paths at 300–3000 K.

$$E_{system} = E_{bond} + E_{over} + E_{under} + E_{val} + E_{pen} + E_{tors} + E_{conj} + E_{vdWaals} + E_{Coulomb} \quad (1)$$

where E_{bond} denotes the bond energy; E_{over} and E_{under} correspond to the over and under coordinated atom in the energy contribution, respectively; and E_{val}, E_{pen}, E_{tors}, E_{conj}, $E_{vdWaals}$, and $E_{Coulomb}$ represent the valence angle term, penalty energy, torsion energy, conjugation effects to energy, nonbonded van der Waals interaction, and Coulomb interaction, respectively.

Two periodic cubic boxes were established. The decomposition process of $C_5F_{10}O$ was simulated; and the dynamic reaction paths, the formation mechanism of the main products and their distribution were systematically analyzed.

Fig. 3 shows the configuration of built models. The box length of $C_5F_{10}O$/air system is 264 Å, which contains 100 $C_5F_{10}O$ molecules, 84 O_2 molecules, and 316 N_2 molecules with a density of 0.00344 g/cm^3. The box length of $C_5F_{10}O$ system is 155 Å, which contains 100 $C_5F_{10}O$ molecules with a density of 0.01186 g/cm^3. The density of each system corresponds to the actual density of gas mixture under 25 °C 0.1 Mpa. To obtain more optimized models, the system was initially minimized using NVE (the number of atoms, volume, and potential energy is constant) ensemble for 5 ps at 5 K, and then equilibrated with the NVT (the number of atoms,volume, and temperature constant) ensemble for 10 ps at 1000 K [19]. Then, the NVT simulations were carried out at different temperatures for 1000 ps with a time step of 0.1 ps to explore the decomposition process of $C_5F_{10}O$. The temperature was controlled by the method of a Berendsen thermostat with a 0.1 ps damping constant [21]. All the ReaxFF-MD simulations in this paper were performed based on the ReaxFF module of ADF (Amsterdam Density Functional) [22].

The DFT calculations were also performed based on the Dmol 3 module of the Materials studio to obtain the influence of temperature and the enthalpy of each decomposition path [23–25]. The reactant and product of each decomposition pathway were geometrically optimized using meta-generalized approximation (mGGA) treated by M06L functions, and the double numerical atomic orbital augmented by d-polarization (DNP) is used as the basis set [26,27]. The energy obtained was corrected from the zero-point energy (ZPE). The frequency analysis was also did to check the stability of each particle and provide temperature corrections on thermodynamic quantities such as enthalpy. And the reaction enthalpy of each decomposition path at different temperatures can be obtained using the following equation,

$$E_{\text{relative}} = E_{products} - E_{\text{reactants}} \quad (1)$$

$$E_{\text{reactants (products)}} = E_{SPE} + E_{ZPE} + E_{\Delta T} \quad (2)$$

where $E_{\text{reactants}}$ and E_{products} represent the energy of reactants and products. E_{SPE}, E_{ZPE}, $E_{\triangle T}$ correspond to the single point energy (SPE), zero point energy and correcting values of enthalpy, respectively.

We also did transition states search using the complete linear synchronous transit (LST) and quadratic synchronous transit (QST) methods for each reaction path to get the reaction activation energy [28].

3. Results and discussion

3.1. Test results

Fig. 4 shows the distribution of the breakdown voltage at different breakdown times and the linear fitting result. The first breakdown voltage of the gas mixture was 27.2 kV; the 30th breakdown voltage was 26.8 kV, which was 0.4 kV lower than the first breakdown voltage. The linear fitting result (R value is 0.6762) shows that the breakdown voltage of the gas mixture decreases with the increase in the breakdown times, indicating that the composition of the gas mixture after repeated breakdown tests has changed. The decomposition products with relatively poor insulation properties were produced, causing the reduction in the breakdown voltage.

Fig. 5 describes the chromatogram of $C_5F_{10}O$/air gas mixture after breakdown test. The qualitative analysis was carried using the National Institute of Standards and Technology database (Nist14.0) and standard

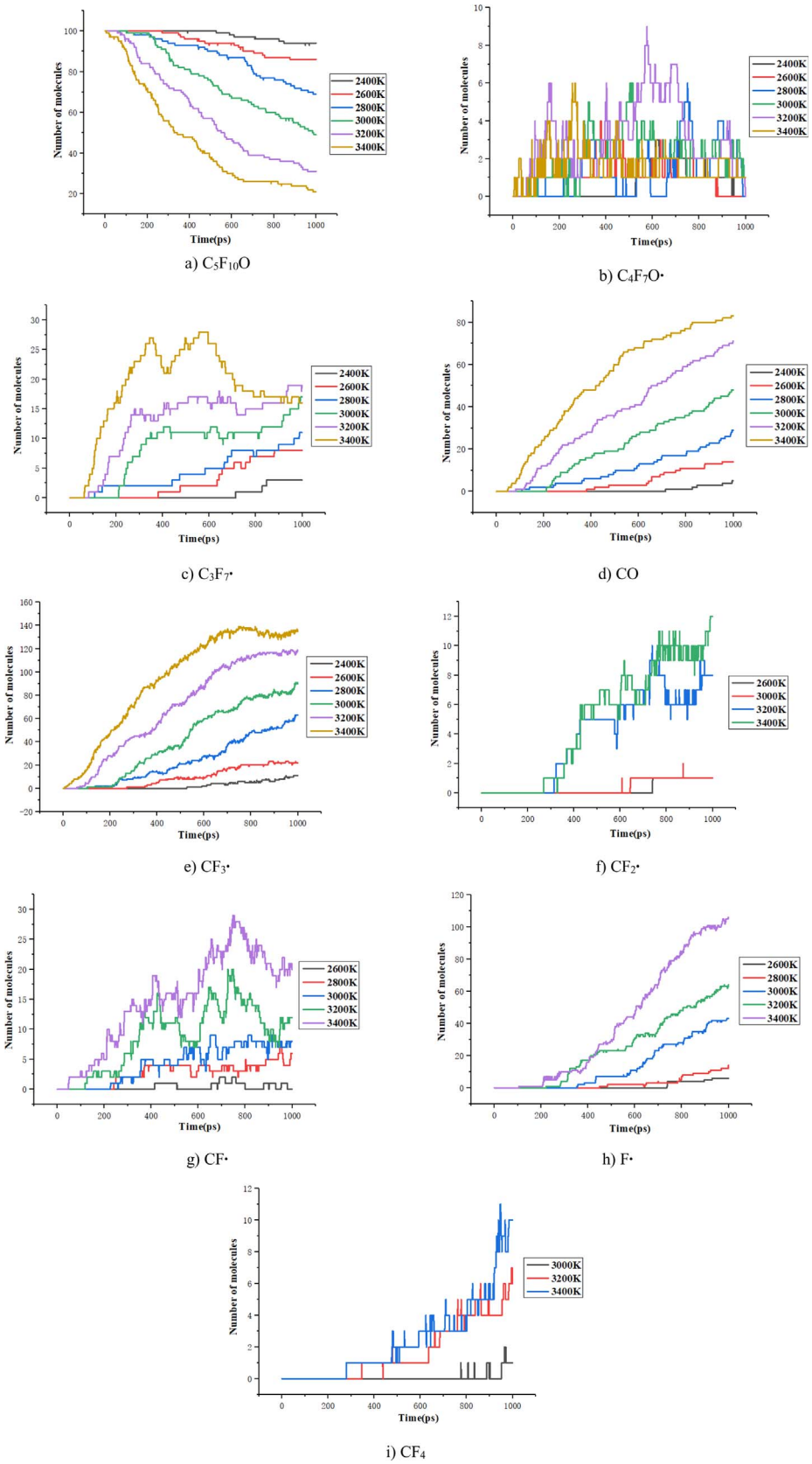

Fig. 9. Time evolution of $C_5F_{10}O$ decomposition products at different temperatures.

gas chromatography. CF_4, C_2F_6, C_3F_8, C_3F_6, C_4F_{10}, CF_2O, C_6F_{14}, and other decomposition products are produced in the $C_5F_{10}O$/air gas mixture after breakdown. Among them, the peak area of CF_4 is the biggest, which indicates that its content is the highest.

We have detected the decomposition products of $C_5F_{10}O/N_2$ gas mixture in our earlier study and found that the content of C_2F_6 is the highest, while CF_2O was not detected [16]. The mass production of CF_2O is related to the addition of oxygen. The O_2 molecules or O· atom

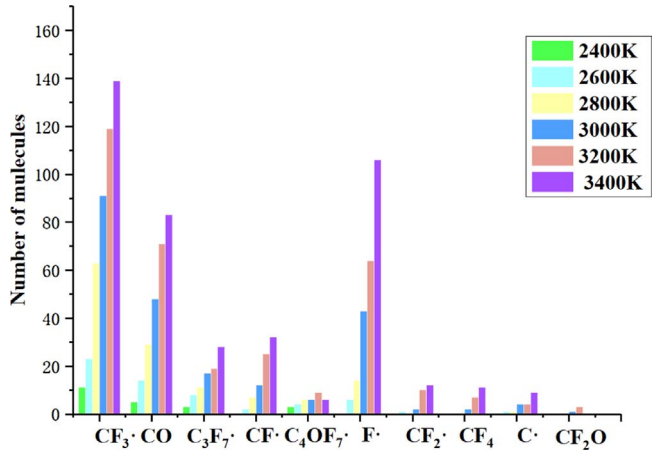

Fig. 10. Maximum number of produced products at different temperatures.

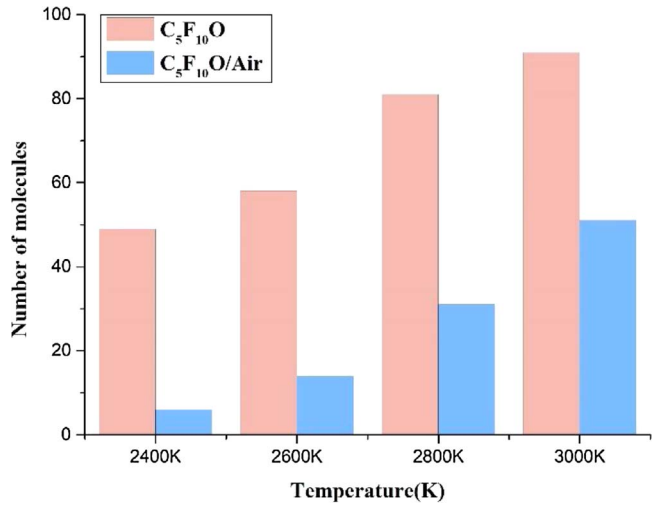

Fig. 11. Final decomposition amount of $C_5F_{10}O$ at different temperatures.

can react with free radicals such as CF_3· generated by $C_5F_{10}O$ under the action of high-energy electric field to form CF_2O.

3.2. Decomposition mechanism of $C_5F_{10}O$/air gas mixture

3.2.1. Decomposition paths of $C_5F_{10}O$/air gas mixture

In order to reveal the decomposition paths of $C_5F_{10}O$/air gas mixture, the reactive molecular dynamics simulations were carried out. It was found that the gas mixture begins to decompose largely at 2600 K. Fig. 6 describes the time evolution of $C_5F_{10}O$/air gas mixture and its major decomposition products at this temperature. The initial generation time and reaction path of each decomposition products can be obtained according to the ReaxFF results. (As shown in Table 1).

According to the simulation results, the main particles and products produced by $C_5F_{10}O$ are C_3F_7CO· (C_4F_7O·), CF_3·, C_3F_7·, CO, CF·, CF_2·, and CF_4. These particles were then optimized at mGGA-M06L level based on the DFT method. The Harmonic vibrational frequencies and total energy of all the species were then calculated to obtain the enthalpy of each reaction path.

$C_5F_{10}O$ began to decompose at 270.625 ps, through path A producing C_4F_7O· and CF_3·, and the reaction needs to absorb 78.71 kcal/mol. At 380 ps, $C_5F_{10}O$ decomposed, producing C_3F_7· and CO through reaction path B, which need to absorb 82.80 kcal/mol. C_4F_7O· decomposed at 414.375 ps, producing CF_3·, CO, and CF·, and this process required to absorb 138.45 kcal/mol. In addition, CF_2· and CF_4 were found at 2600 K and 3000 K, which were formed by the decomposition of CF_3· or combination of CF_3· with F·. It should be noted that the direct $C_5F_{10}O$ decomposition pathways belong to bond-cleavage reactions. And these bond-cleavage reactions are determined as barrierless without transition states using the complete LST and QST methods. Fig. 7 shows the relative energy of each decomposition path. We can find that there are two main decomposition paths of $C_5F_{10}O$ (path A and B), producing C_4F_7O·, CF_3·, C_3F_7·, CO, and other particles.

Fig. 8 shows the enthalpy change of the main decomposition paths with temperature from 300–3000 K. The enthalpy of the paths A, B, and C decreases significantly as the temperature increases, indicating that the reaction is more likely to occur; that is, the increase in temperature contributes to the decomposition of $C_5F_{10}O$. In addition, the enthalpy of path D did not change significantly with temperature, indicating that the increase in temperature had little effect on the formation of CF_2·.

3.2.2. Production distribution at different temperatures

At present, the $C_5F_{10}O$/air gas mixture is mainly used in engineering applications, in which the content of $C_5F_{10}O$ is generally less than 20% [8].Therefore, the $C_5F_{10}O$/air gas mixture model with a mixing ratio of 2:8 is constructed. Partial discharge (corona discharge) and arc discharge are the two most common types of discharges in electrical equipment. The temperature in the core region of arc discharge and corona discharge is 3000–12,000 K, and 700–1200 K, respectively [28–29]. The reactive molecular dynamics simulations of $C_5F_{10}O$/air gas mixture system were then carried out to reveal the decomposition mechanism at different temperatures.

Fig. 9 shows time evolution of $C_5F_{10}O$ decomposition products with temperature from 2400 K to 3400 K. The decomposition rate of $C_5F_{10}O$/air gas mixture significantly accelerated with the increase of temperature. For example, only 6 $C_5F_{10}O$ molecules decomposed at the end of the simulation at 2400 K, and 79 $C_5F_{10}O$ molecules are decomposed at 3400 K. When the temperature is below 2800 K, the decomposition amount of $C_5F_{10}O$ at the end of simulation is below 50%.

Table 2
Final amount of decomposition products at different temperatures.

Major species	Temperature							
	2400 K		2600 K		2800 K		3000 K	
	$C_5F_{10}O$	$C_5F_{10}O$/air	$C_5F_{10}O$	$C_5F_{10}O$/air	$C_5F_{10}O$	$C_5F_{10}O$/air	$C_5F_{10}O$	$C_5F_{10}O$/air
CF_3·	32	11	86	23	142	63	151	91
CO	13	5	45	14	72	29	82	48
C_3F_7·	7	3	18	8	21	11	37	17
CF·	6	0	30	2	60	7	74	12
C_4F_7O·	3	3	6	4	11	6	18	6
F·	0	0	16	6	48	14	74	43
CF_2·	0	0	9	0	24	0	19	2
CF_4	0	0	7	0	49	0	57	2
C·	0	0	7	1	38	1	42	4

The maximum number of produced products at different temperatures is given in Fig. 10. The maximum number of $C_4F_7O\cdot$, $CF_3\cdot$, $C_3F_7\cdot$, CO, $CF\cdot$, $CF_2\cdot$, and CF_4 increased with the increase in temperature. The content of $CF_3\cdot$ in different temperature conditions is the highest among all the products, followed by CO and $F\cdot$. In addition, since air contains a certain amount of oxygen, the formation of CF_2O occurred during the simulation process.

According to the results shown in Fig. 10, the contents of $F\cdot$ and CO increase as the reaction progress at different temperatures. The $C_4F_7O\cdot$ produced by the decomposition of $C_5F_{10}O$ is irregular with the reaction time, especially at the temperature of 3000 K. At the beginning of the reaction, a large amount of $C_4F_7O\cdot$ is produced, but the content of this product is maintained at a relatively stable level after 100 ps. This may be related to the existence of a certain dynamic balance between the generation and decomposition of $C_4F_7O\cdot$ during the decomposition process. The content of $CF\cdot$, $CF_2\cdot$, $F\cdot$, and CF_4 increased with the reaction progress at different temperatures, and the production rate increased with the temperature. Among these products, $F\cdot$ and CF_4 showed rapid growth trend at temperatures above 2800 K. The content of $C_3F_7\cdot$ showed a tendency to increase first and then decrease under the condition of 3400 K, indicating that the high temperature caused the decomposition of $C_3F_7\cdot$. In addition, the yield and rate of three free radicals of $CF_2\cdot$, $CF\cdot$, and CF_4 in $C_5F_{10}O$/air system began to increase dramatically at temperatures above 3000 K; while under 3000 K, the contents were low. The generation rate of $CF_3\cdot$ slowed down after 600 ps at 3200 K and 3400 K. This trend is due to the combination of $CF_3\cdot$ and $F\cdot$, which produces a large amount of CF_4 and consumes $CF_3\cdot$ and $F\cdot$ in the system.

Actually, electron collision ionization, thermal decomposition and photoionization are the main factors leading to the decomposition of gas in a discharge. Under the condition of arc or spark discharge, the dissociation of gas molecules is mainly caused by electron collision ionization or high temperature. Under the condition of partial discharge or corona discharge, the dissociation of gas molecules is mainly caused by electron collision ionization due to the low temperature of the discharge area. And the type and relative content of particles generated by the discharge will determine the composition of the decomposition products to a certain extent. According to the simulation results, $C_5F_{10}O$/air gas mixture mainly produces $CF_3\cdot$, $F\cdot$, CO and $C_3F_7\cdot$ at high temperature. The breakdown tests shows that CF_4, C_2F_6, C_3F_8, C_3F_6, C_4F_{10}, CF_2O, C_6F_{14} were generated. And the formation of these products needs the participation of $CF_3\cdot$, $F\cdot$ and $C_3F_7\cdot$. Thus the results of ReaxFF are consistent with breakdown experiments.

3.2.3. Effect of air on the decomposition of $C_5F_{10}O$

In order to investigate the effect of air on the decomposition of $C_5F_{10}O$, we carried out simulations for pure $C_5F_{10}O$ system at 2400–3000 K. Fig. 11 shows the comparison of the decomposition of $C_5F_{10}O$ and $C_5F_{10}O$/air gas mixture at the same temperature. There are 49 $C_5F_{10}O$ molecules decomposed in the $C_5F_{10}O$ system at 2400 K, and only 6 $C_5F_{10}O$ molecules decomposed in $C_5F_{10}O$/air gas mixture system. The decomposition amount of $C_5F_{10}O$ reached 91 in the $C_5F_{10}O$ system at 3000 K, while only 51 $C_5F_{10}O$ molecules decomposed in the gas mixture system.

Table 2 shows the final amount of $C_5F_{10}O$ decomposition products at different temperatures. The production of the main products in $C_5F_{10}O$/air gas mixture system at the same temperature is significantly lower than that of the pure $C_5F_{10}O$ system. The content of $C_3F_7\cdot$, $CF\cdot$, $C_4F_7O\cdot$, $CF_2\cdot$, CF_4, and $C\cdot$ significantly reduced, which effectively protected the insulation strength of the system without damage. In fact, the addition of air leads to the decrease in density under the same pressure, and the concentration of $C_5F_{10}O$ in the system is reduced. The addition of air prevents the high-energy particles from colliding directly with $C_5F_{10}O$ molecules to a certain extent, which is beneficial to the system insulation. Therefore, the $C_5F_{10}O$/air gas mixture is suitable for using as a gas-insulated medium. And the synergistic effect between $C_5F_{10}O$ and air needs further study.

3.3. Environmental effects of $C_5F_{10}O$/air gas mixture

As mentioned above, $C_5F_{10}O$ exhibits very low GWP compared to SF_6 and the GWP value of $C_5F_{10}O$ gas mixture with the molar fraction lower than 20% is less than 0.7 [16]. And it does not contribute to ozone depletion. The atmospheric degradation of $C_5F_{10}O$ does not lead to the generation of long chain acids that are of environmental concern [14].

The decomposition products of $C_5F_{10}O$, such as CF_4, C_2F_6, C_3F_8, C_4F_{10} and C_6F_{14} belong to Perfluorocarbons. The GWP values of these substances are 7390, 12200, 8830, 8860 and 9300, which is higher than $C_5F_{10}O$. It should be noted that the concentration of decomposition products is relatively low under normal working and even fault conditions. Hyrenbach et al. detected the composition of $C_5F_{10}O$/air gas mixture used in the switch cabinet and found that the content of CF_4, C_2F_6, C_3F_8, C_4F_{10} and C_3F_6 under arc discharge is at ppm level. The max concentration of CF_4, C_2F_6, C_3F_8, C_4F_{10} and C_3F_6 is 100 ppm, 10 ppm, 19 ppm, 2 ppm and 14 ppm, respectively [14]. Therefore using $C_5F_{10}O$/air gas mixture can effectively reduce emissions.

4. Conclusion

In this paper, the insulation and decomposition characteristics of environment-friendly alternative gas $C_5F_{10}O$/air gas mixture were studied experimentally and theoretically. First, the breakdown test of $C_5F_{10}O$/air gas mixture was carried out using the gas insulation performance test platform, and the components after the test were detected by GC-MS. Then the decomposition mechanism of $C_5F_{10}O$/air gas mixture under different temperature conditions are revealed comprehensively by using the method of reactive molecular dynamics and density functional theory. The main decomposition path, the by-products, and their distribution were analyzed.

There are two main decomposition paths of $C_5F_{10}O$ producing $C_4F_7O\cdot$, $CF_3\cdot$, $C_3F_7\cdot$, CO, and other particles. With temperature increase, the decomposition rate of $C_5F_{10}O$ accelerates, and further produce $CF_2\cdot$, $CF\cdot$, $F\cdot$, CF_4, C_2F_6, C_3F_8, and other decomposition products. Also, the breakdown voltage of the gas mixture decreases with the increase in the breakdown times. CF_4, C_2F_6, C_3F_8, C_3F_6, C_4F_{10}, CF_2O, C_6F_{14} are detected in the $C_5F_{10}O$/air gas mixture after breakdown. And the generation of CF_2O is relative to the existence of oxygen.

Acknowledgement

The current work is supported by the Science and Technology Project of China Southern Power Grid (No. ZBKJXM20170090)

References

[1] M. Rabie, C.M. Franck, An assessment of eco-friendly gases for electrical insulation to replace the most potent industrial greenhouse gas SF_6, Environ. Sci. Technol. 52 (2018) 369–380, http://dx.doi.org/10.1021/acs.est.7b03465.
[2] M.P. Sulbaek Andersen, M. Kyte, S.T. Andersen, C.J. Nielsen, O.J. Nielsen, Atmospheric chemistry of $(CF_3)_2CF-C\equiv N$: a replacement compound for the most potent industrial greenhouse gas, SF_6, Environ. Sci. Technol. 51 (2017) 1321–1329, http://dx.doi.org/10.1021/acs.est.6b03758.
[3] Y. Wu, C. Wang, H. Sun, M. Rong, A.B. Murphy, T. Li, J. Zhong, Z. Chen, F. Yang, C. Niu, Evaluation of SF_6-alternative gas C5-PFK based on arc extinguishing performance and electric strength, J. Phys. D Appl. Phys. 50 (2017), http://dx.doi.org/10.1088/1361-6463/aa800b.
[4] R. Ullah, A. Rashid, F. Khan, A. Qadeer, Dielectric characteristic of dichlorodifluoromethane (R12) gas and mixture with N_2/air as an alternative to SF_6 gas, High Volt. 2 (2017) 205–210.
[5] J. Reilly, R. Prinn, J. Harnisch, J. Fitzmaurice, H. Jacoby, D. Kicklighter, J. Melillo, P. Stone, A. Sokolov, C. Wang, Multi-gas assessment of the Kyoto protocol, Nature 401 (1999) 549–555, http://dx.doi.org/10.1038/44069.
[6] B. Obama, The irreversible momentum of clean energy, Science 355 (80) (2017) 126–129, http://dx.doi.org/10.1126/science.aam6284.
[7] Y. Kieffel, T. Irwin, P. Ponchon, J. Owens, Green gas to replace SF_6 in electrical

grids, IEEE Power Energy Mag. 14 (2016) 32–39, http://dx.doi.org/10.1109/MPE.2016.2542645.
[8] M. Hyrenbach, S. Zache, Alternative insulation gas for medium-voltage switchgear, PCIC Eur. Pet. Chem. Ind. Conf. Eur. Conf. Proceedings (2016), http://dx.doi.org/10.1109/PCICEurope.2016.7604648.
[9] J.D. Mantilla, N. Gariboldi, S. Grob, M. Claessens, Investigation of the insulation performance of a new gas mixture with extremely low GWP, EIC 2014 - Proc. 32nd Electr. Insul. Conf. (2014) 469–473, http://dx.doi.org/10.1109/EIC.2014.6869432.
[10] P. Simka, N. Ranjan, Dielectric strength of C5 perfluoroketone, 19th Int. Symp. High Volt. Eng. (2015), pp. 23–28.
[11] F. Zeng, J. Tang, Y. Xie, Q. Zhou, C. Zhang, Experimence study of trace water and oxygen impact on SF_6 decomposition characteristics under partial discharge, J. Electr. Eng. Technol. 10 (2015) 1787–1796, http://dx.doi.org/10.5370/JEET.2015.10.4.1787.
[12] A.V. Tatarinov, I.V. Bilera, V.A. Shakhatov, S.V. Shakhatov, P. Avtaeva, V. Solomakhin, R. Maladen, C. Prévé, D. Piccoz, Comparative study of degradation of trans -1,3,3,3-trifluoropropene, 2,3,3,3-tetrafluoropropene, perfluoro-3-methylbutanone-2, and sulfur hexafluoride in dielectric-barrier discharge, High Energy Chem. 50 (2016) 64–70.
[13] A.V. Tatarinov, I.V. Bilera, S.V. Avtaeva, V.A. Shakhatov, P.V. Solomakhin, R. Maladen, C. Prévé, D. Piccoz, Dielectric barrier discharge processing of trans−CF_3CH=CHF and $CF_3C(O)CF(CF_3)_2$, their mixtures with air, N_2, CO_2 and analysis of their decomposition products, Plasma Chem. Plasma Process. 35 (2015) 845–862, http://dx.doi.org/10.1007/s11090-015-9635-8.
[14] M. Hyrenbach, T.A. Paul, J. Owens, Environmental and safety aspects of airplus insulated, GIS CIRED 24th Int. Conf. Elect. Distr (2017).
[15] S. Xiao, Y. Li, X. Zhang, S. Tian, Z. Deng, J. Tang, Effects of micro-water on decomposition of the environment-friendly insulating medium $C_5F_{10}O$, AIP Adv. 7 (2017), http://dx.doi.org/10.1063/1.4990512.
[16] X. Zhang, Y. Li, S. Xiao, J. Tang, S. Tian, Z. Deng, Decomposition mechanism of $C_5F_{10}O$: an environmentally friendly insulation medium, Environ. Sci. Technol. 51 (2017) 10127–10136, http://dx.doi.org/10.1021/acs.est.7b02419.
[17] X. Zhang, Y. Li, S. Tian, S. Xiao, D. Chen, J. Tang, R. Zhuo, Decomposition mechanism of the C5-PFK/CO_2 gas mixture as an alternative gas for SF_6, Chem. Eng. J. 336 (2018) 36–48.
[18] K. Chenoweth, A.C.T. van Duin, P. Persson, M.-J. Cheng, J. Oxgaard, W.A. Goddard III, Development and application of a ReaxFF reactive force field for oxidative dehydrogenation on vanadium oxide catalysts, J. Phys. Chem. C 112 (2008) 14645–14654, http://dx.doi.org/10.1021/jp802134x.
[19] D. Hong, L. Liu, Y. Huang, C. Zheng, X. Guo, Chemical effect of H_2O on CH_4 oxidation during combustion in O_2/H_2O environments, Energy Fuels (2016), http://dx.doi.org/10.1021/acs.energyfuels.6b01360 acs.energyfuels.6b01360.
[20] A.C.T. Van Duin, S. Dasgupta, F. Lorant, W.A. Goddard, ReaxFF: a reactive force field for hydrocarbons, J. Phys. Chem. A 105 (2001) 9396–9409, http://dx.doi.org/10.1021/jp004368u.
[21] H.J.C. Berendsen, J.P.M. Postma, W.F. Van Gunsteren, A. Dinola, J.R. Haak, Molecular dynamics with coupling to an external bath, J. Chem. Phys. 81 (1984) 3684–3690, http://dx.doi.org/10.1063/1.448118.
[22] G. te Velde, F.M. Bickelhaupt, E.J. Baerends, C. Fonseca Guerra, S.J.A. van Gisbergen, J.G. Snijders, T. Ziegler, Chemistry with ADF, J. Comput. Chem. 22 (2001) 931–967, http://dx.doi.org/10.1002/jcc.1056.
[23] K.M. Murali, S. Baskaran, M.N. Arumugham, Photochemical and DFT/TD-DFT study of trifluoroethoxy substituted asymmetric metal-free and copper(II) phthalocyanines, J. Fluor. Chem. 202 (2017) 1–8, http://dx.doi.org/10.1016/j.jfluchem.2017.08.011.
[24] S. Emamian, Toward understanding regioselectivity and molecular mechanism in the synthesis of CF2H-containing 2-pyrazolines: a molecular electron-density theory study, J. Fluor. Chem. 199 (2017) 77–91, http://dx.doi.org/10.1016/j.jfluchem.2017.05.004.
[25] A. Wang, Y. Zhao, X. Liu, L. Chang, X. Xuan, 1,3-Bis(carboxymethyl)imidazolium bis(trifluoromethylsulfonyl)imide organic salt: synthesis, single crystal structure, vibrational spectra, DFT calculations and physical-chemical properties, J. Fluor. Chem. 186 (2016) 7–11, http://dx.doi.org/10.1016/j.jfluchem.2016.04.003.
[26] Y. Zhao, D.G. Truhlar, The M06 suite of density functionals for main group thermochemistry, thermochemical kinetics, noncovalent interactions, excited states, and transition elements: two new functionals and systematic testing of four M06-class functionals and 12 other functionals, Theor. Chem. Acc. 120 (2008) 215–241, http://dx.doi.org/10.1007/s00214-007-0310-x.
[27] Y. Zhao, D.G. Truhlar, A new local density functional for main-group thermochemistry, transition metal bonding, thermochemical kinetics, and noncovalent interactions, J. Chem. Phys. 125 (2006), http://dx.doi.org/10.1063/1.2370993.
[28] T.A. Halgren, W.N. Lipscomb, The synchronous-transit method for determining reaction pathways and locating molecular transition states, Chem. Phys. Lett. 49 (1977) 225–232, http://dx.doi.org/10.1016/0009-2614(77)80574-5.
[29] R. Ono, T. Oda, Measurement of gas temperature and OH density in the afterglow of pulsed positive corona discharge, J. Phys. D Appl. Phys. 41 (2008), http://dx.doi.org/10.1088/0022-3727/41/3/035204.